Possible planet formation in the young, low-mass, multiple stellar system GG Tau A

Article *in* Nature · October 2014

DOI: 10.1038/nature13822 · Source: PubMed

14 authors, including:

Emmanuel Di Folco
University of Bordeaux
99 PUBLICATIONS **1,775** CITATIONS
SEE PROFILE

Stephane Guilloteau
French National Centre for Scientific Research
252 PUBLICATIONS **4,139** CITATIONS
SEE PROFILE

Yann Boehler
Rice University
12 PUBLICATIONS **187** CITATIONS
SEE PROFILE

Jeffrey S. Bary
Colgate University
29 PUBLICATIONS **278** CITATIONS
SEE PROFILE

LETTER

doi:10.1038/nature13822

Possible planet formation in the young, low-mass, multiple stellar system GG Tau A

Anne Dutrey[1,2], Emmanuel Di Folco[1,2], Stéphane Guilloteau[1,2], Yann Boehler[3], Jeff Bary[4], Tracy Beck[5], Hervé Beust[6], Edwige Chapillon[1,7], Frédéric Gueth[7], Jean-Marc Huré[1,2], Arnaud Pierens[1,2], Vincent Piétu[7], Michal Simon[8] & Ya-Wen Tang[9]

The formation of planets around binary stars may be more difficult than around single stars[1–3]. In a close binary star (with a separation of less than a hundred astronomical units), theory predicts the presence of circumstellar disks around each star, and an outer circumbinary disk surrounding a gravitationally cleared inner cavity around the stars[4,5]. Given that the inner disks are depleted by accretion onto the stars on timescales of a few thousand years, any replenishing material must be transferred from the outer reservoir to fuel planet formation (which occurs on timescales of about one million years). Gas flowing through disk cavities has been detected in single star systems[6]. A circumbinary disk was discovered around the young low-mass binary system GG Tau A (ref. 7), which has recently been shown to be a hierarchical triple system[8]. It has one large inner disk[9] around the single star, GG Tau Aa, and shows small amounts of shocked hydrogen gas residing within the central cavity[10], but other than a single weak detection[11], the distribution of cold gas in this cavity or in any other binary or multiple star system has not hitherto been determined. Here we report imaging of gas fragments emitting radiation characteristic of carbon monoxide within the GG Tau A cavity. From the kinematics we conclude that the flow appears capable of sustaining the inner disk (around GG Tau Aa) beyond the accretion lifetime, leaving time for planet formation to occur there. These results show the complexity of planet formation around multiple stars and confirm the general picture predicted by numerical simulations.

The triple stellar system GG Tau A consists of a single star GG Tau Aa and a close binary GG Tau Ab (with individual stars named Ab1 and Ab2). The system is 1–5 million years old[12,13], and is located 140 pc from Earth in a hole of the Taurus molecular cloud. Its molecular emission is free of contamination[14] and there is no known outflow or jet associated with the source. GG Tau Aa and Ab have an apparent separation of 35 astronomical units (AU) while the separation of GG Tau Ab1 and Ab2 is 4.5 AU (ref. 8). The outer Keplerian disk of gas and dust surrounding GG Tau A (called the circumbinary disk for simplicity) consists of a ring extending from radius $r \approx 190$ AU to $r \approx 280$ AU and an outer disk extending up to 800 AU from the central stars with a total mass of $\sim 0.15 M_{\odot}$ (ref. 14; here $M_{\odot}$ is the solar mass).

Using the Atacama Large Millimetre Array (ALMA), we observed GG Tau A in the dust thermal emission at 0.45 mm wavelength and in the CO $J = 6$–5 line (Fig. 1a–c) with an angular resolution of $\theta \approx 0.25''$ or ~35 AU. The continuum image shows cold dust emission from only one circumstellar disk-like structure associated with GG Tau Aa[9,15]. We estimate the minimum dust disk size to be ~7 AU while the minimum mass of gas and dust is roughly $10^{-3} M_{\odot}$, about Jupiter's mass. The complex CO $J = 6$–5 spectral line shape at the location of GG Tau Aa also reveals the existence of a CO circumstellar disk of outer radius ~20 AU (Methods and Extended Data Fig. 1). We do not detect cold dust emission around GG Tau Ab, even though the existence of an inner dust disk (or disks) has been inferred from unresolved infrared emission[16]. Our 0.45-mm flux upper limits (Methods) are compatible with tidal truncation, which would prevent any circumstellar disk extending beyond about 2 AU (ref. 8). The ALMA CO $J = 6$–5 image (Fig. 1a–c and Extended Data Figs 1 and 2) also clearly resolves CO gas within the central cavity with a structure indicative of the streamer-like features which have been hinted at by hydrodynamic simulations in binary systems[5,17]. The CO gas appears to be inhomogeneous, existing as a series of fragments, and the structure is dominated by an east–west extension. No northern feature is seen, contrary to the very low level (a signal-to-noise ratio of 2) extension seen in continuum at 270 GHz (ref. 15).

The Institut de RadioAstronomie Millimetrique (IRAM) image (Fig. 1d–f and Extended Data Fig. 2) reveals, at lower angular resolution, that the CO $J = 2$–1 emission peaks are located near the inner edge of the outer ring (at radius ~100–150 AU). In contrast, the CO $J = 6$–5 emission peaks near GG Tau Aa and GG Tau Ab, close to the bright regions of near-infrared $v = 1$–0 S(1) H_2 emission (Fig. 1c) that have been interpreted as shock-excited gas at the interface between the streamer and gas associated with the inner disks[10]. A study of the excitation conditions (Methods) reveals that CO $J = 2$–1 and $J = 6$–5 emissions arise in different physical conditions: the former correspond to extended, cold (~35 K) optically thick areas, while the latter trace optically thin, warmer gas (~70 K) particularly at the interface between the streamer and the inner disk of Aa. The mass of each CO $J = 6$–5 fragment is about $5 \times 10^{-5} M_{\odot}$ (Methods). With a minimum accretion rate of $10^{-8} M_{\odot}\,\mathrm{yr}^{-1}$, a fragment reaching the Aa disk may disappear in at most 5,000 years (a few tens of times the orbital period of the binary Aa–Ab). The Aa disk mass currently represents about 20 such fragments; in 1 Myr, at least 200 fragments of similar mass must have been accreted to sustain such a disk. The corresponding minimum mass, which accreted from the circumbinary disk, represents about 10% of the current outer disk mass ($\sim 0.15 M_{\odot}$). The morphology of the gas in the CO $J = 6$–5 and $J = 2$–1 maps reveals departures from symmetry, unlike hydrodynamical simulations which predict symmetric streamers for an equal-mass, low-eccentricity binary system[5]. GG Tau Aa and Ab each have a mass of about $0.65 M_{\odot}$ (ref. 13) and their orbital eccentricity is constrained to $e \leq 0.35$ (ref. 18). The origin of this asymmetry might either be found in this eccentricity[19,20] or in the triple nature of GG Tau A, as the binarity of Ab breaks the symmetry.

The change in velocity of the CO $J = 6$–5 emission along the major axis of the dust ring is similar to that of CO $J = 2$–1 (Fig. 1b, e and Extended Data Figs 1 and 2) and the velocity gradient is that of a rotating disk[14,21]. At radius 200 AU, we find that the velocity of the CO $J = 6$–5 gas agrees with the known Keplerian speed (Methods and Extended Data Table 1) derived from existing ^{13}CO maps[14,21] and corresponds to the canonical dynamical mass of the triple star GG Tau A ($1.28 M_{\odot}$)[14,21]. This is still true down to a radius of ~70–80 AU. Closer to the stars, the velocity pattern of the CO $J = 6$–5 emission becomes dominated by the individual gravitational fields of GG Tau Aa and GG Tau Ab. Limited

[1]Université de Bordeaux, LAB, UMR 5804, F-33270 Floirac, France. [2]Centre National de la Recherche Scientifique (CNRS), LAB, UMR 5804, F-33270 Floirac, France. [3]Centro de Radioastronomia y Astrofisica (CRyA), University of Mexico, Apartado Postal 3-72, 58089 Morelia, Michoacan, Mexico. [4]Department of Physics and Astronomy, Colgate University, 13 Oak Drive, Hamilton, New York 13346, USA. [5]Space Telescope Science Institute, 3700 San Martin Drive, Baltimore, Maryland 21218, USA. [6]Institut de Planetologie et d'Astrophysique de Grenoble (IPAG), UMR 5274, BP 53, F-38041 Grenoble Cedex 9, France. [7]Institut de RadioAstronomie Millimetrique (IRAM), 300 rue de la Piscine, F-38046 Saint Martin d'Hères, France. [8]Stony Brook University, Stony Brook, New York 11794-3800, USA. [9]Academia Sinica Institute of Astronomy and Astrophysics, PO Box 23-141, Taipei 106, Taiwan.

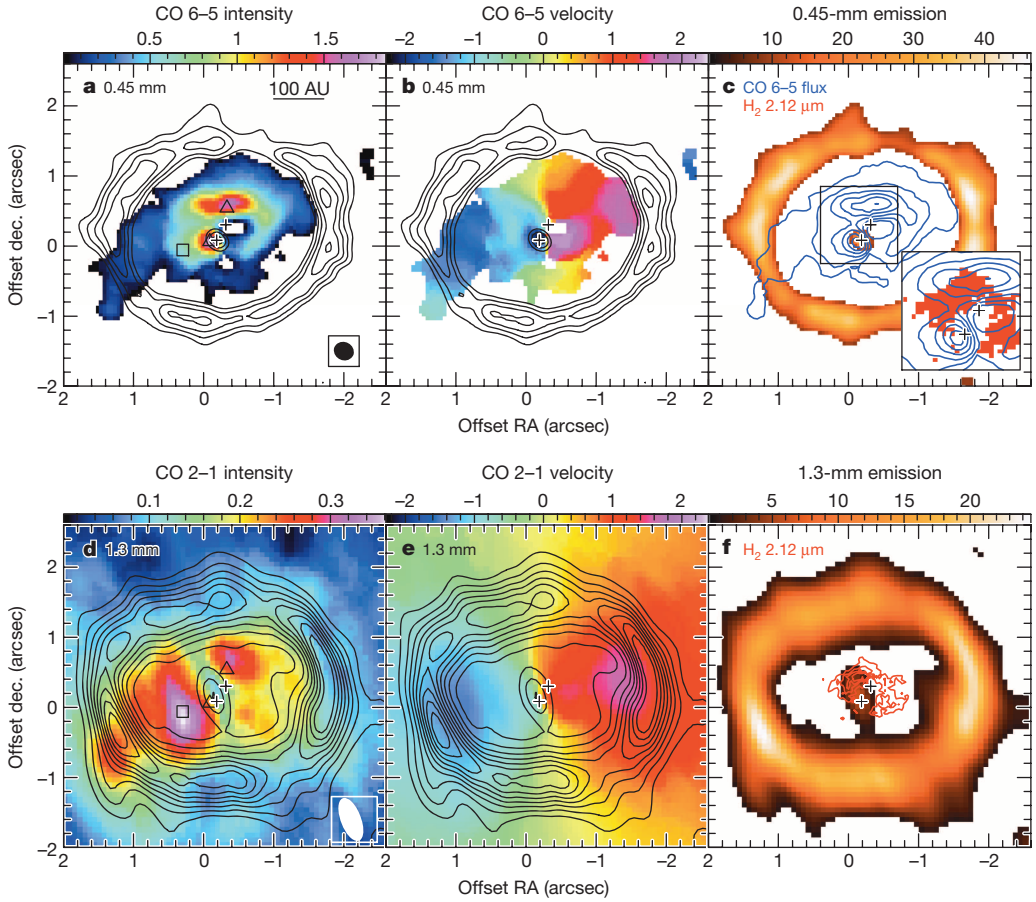

Figure 1 | ALMA and IRAM images of GG Tau A. **a**–**c**, ALMA; **d**–**f**, IRAM. **a**, 0.45-mm emission (black contours) and CO 6–5 flux (colour: see colour scale at top). **b**, 0.45-mm emission (black contours) and CO velocity field (colour). **c**, 0.45-mm emission (colour) with CO 6–5 flux (blue contours) and in inset H_2 intensity (red). **d**, **e**, as **a**, **b**, but for 1.3-mm emission (contours) and CO 2–1 flux (colour). **f**, 1.3-mm emission (colour) and H_2 intensity (contours). Positions are relative to right ascension (RA) 04 h 32 min 30.359 s and declination (dec.) 17° 31′ 40.38″ (J2000). Crosses are the locations of Aa (south) and Ab (north) components, and triangles and squares show the locations of the CO $J = 6–5$ and $J = 2–1$ peaks, respectively. Units on the colour scales are Jy per beam km s^{-1} (**a**, **d**), km s^{-1} (**b**, **e**) and mJy per beam (**c**, **f**). In **a** and **d**, the beam size is given in the inset.

angular resolution (35 AU) precludes detailed kinematical analysis, but study of the northern CO $J = 6–5$ peak vicinity reveals that its velocity gradient is dominated by rotation, with departure from rotation compatible with infall motion (Methods and Extended Data Fig. 3).

Another result concerns the dust and gas circumbinary reservoir. The dust emission from the circumbinary ring is very well resolved (Fig. 1 and Extended Data Fig. 4) but appears uniform within the noise. The combination of the 0.45-mm ALMA image with existing 1.3- and 3.4-mm continuum maps[14,21] allows for a direct measurement of the radial dependence of the temperature in the circumbinary dust disk. Using a radiative transfer model (Methods), we determined the dust temperature profile $T_D(r) = 13.8 \times (r/200\ \mathrm{AU})^{-1.1}$ K, which gives a temperature of ~8.5 K at 300 AU. Thanks to the 0.45-mm image, the derived dust temperature is almost independent of the dust properties. This represents a significant improvement on the knowledge of the mid-plane physical conditions (Methods, Extended Data Table 2 and Extended Data Fig. 4). Since our measurement is the result of vertical averaging of the temperature, and the upper layers of the disk are hotter owing to direct irradiation by the stellar ultraviolet flux, the mid-plane must be even colder. The limited grain growth (Methods) helps explain the low temperature, since small grains are most efficient at attenuating ultraviolet radiation coming from the central stars. Furthermore, at the ring inner edge, a puffed-up rim, caused by direct stellar heating, should cast a shadow on the outer region of the disk. Such a shielding effect could explain the steep slope of the temperature profile. Previous ^{13}CO measurements and analysis yielded a similarly steep slope (exponent ~0.9) for the gas temperature profile in the circumbinary disk but a warmer gas temperature (~ 20 K, at 300 AU)[21]. This is consistent with CO molecules being trapped onto grains in the mid-plane, whose temperature is below the CO freeze-out point (~17 K), and with CO gas only present in the heated upper layers of the disk[22].

Figure 1 shows that, unlike the continuum emission of dust, little CO $J = 6–5$ line emission is detected near the circumbinary disk inner radius at ~200–250 AU. This could be attributable to both an H_2 density insufficient to thermalize the upper energy level of the CO transition and lower sensitivity of the interferometer to relatively large angular scale (>1″) structure (Methods). Figure 1 also shows strong excess of CO $J = 6–5$ and 2–1 emission at position angle ~120° (measured east of north) and radius ~240–270 AU. From these CO data alone we cannot discriminate between a temperature and/or density increase (Methods). We suggest that this localized emission is attributable to a progenitor of a sub-stellar body reminiscent of the planetary-mass companion imaged around the low-mass binary 2MASS 0103AB[23]. Such a companion would provide a natural explanation for the confinement of ~80% of the circumbinary mass within the ~90 AU breadth of the ring[21]. Simulations of the evolution of binary systems in which Kepler detected exoplanets demonstrate that Saturn-mass proto-planets can remain at the ring outer edge in some cases[20]. We do not, however, detect a gap near the outer edge of the gas and dust circumbinary ring but existing ^{12}CO, ^{13}CO and thermal dust images are not incompatible with its existence (Methods).

Our observations demonstrate that active replenishment from the outer disk can sustain the circumstellar disk surrounding GG Tau Aa for a time exceeding the accretion lifetime, increasing its potential for planet formation. The presence of a condensation at the outer edge of

the ring is puzzling, and needs further investigation to determine its links with accretion processes and possible planet formation. Since almost half of Sun-like stars were born in multiple systems[24], our observations provide a step towards understanding the true complexity of protoplanetary disks in multiple stellar systems and unveiling planet formation mechanisms for a significant fraction of stellar systems in our Galaxy.

Online Content Methods, along with any additional Extended Data display items and Source Data, are available in the online version of the paper; references unique to these sections appear only in the online paper.

Received 19 March; accepted 1 September 2014.

1. Nelson, A. F. Planet formation is unlikely in equal-mass binary systems with A ~ 50 AU. *Astrophys. J.* **537,** L65–L68 (2000).
2. Mayer, L., Wadsley, J., Quinn, T. & Stadel, J. Gravitational instability in binary protoplanetary discs: new constraints on giant planet formation. *Mon. Not. R. Astron. Soc.* **363,** 641–648 (2005).
3. Thébault, P., Marzari, F. & Scholl, H. Relative velocities among accreting planetesimals in binary systems: the circumprimary case. *Icarus* **183,** 193–206 (2006).
4. Artymowicz, P. & Lubow, S. H. Dynamics of binary-disk interaction. 1: Resonances and disk gap sizes. *Astrophys. J.* **421,** 651–667 (1994).
5. Bate, M. R. & Bonnell, I. A. Accretion during binary star formation — II. Gaseous accretion and disc formation. *Mon. Not. R. Astron. Soc.* **285,** 33–48 (1997).
6. Casassus, S. *et al.* Flows of gas through a protoplanetary gap. *Nature* **493,** 191–194 (2013).
7. Skrutskie, M. F. *et al.* Detection of circumstellar gas associated with GG Tauri. *Astrophys. J.* **409,** 422–428 (1993).
8. Di Folco, E. *et al.* GG Tauri: the fifth element. *Astron. Astrophys.* **565,** L2 (2014).
9. Andrews, S. M. *et al.* Resolved multifrequency radio observations of GG Tau. *Astrophys. J.* **787,** 148 (2014).
10. Beck, T. L. *et al.* Circumbinary gas accretion onto a central binary: infrared molecular hydrogen emission from GG Tau A. *Astrophys. J.* **754,** 72 (2012).
11. Guilloteau, S. & Dutrey, A. G. G. in *The Formation of Binary Stars* (eds Zinnecker, H. & Mathieu, R.) 229–233 (IAU Symposium, Vol. 200, 2001).
12. Hartigan, P. & Kenyon, S. J. A spectroscopic survey of subarcsecond binaries in the Taurus-Auriga dark cloud with the Hubble Space Telescope. *Astrophys. J.* **583,** 334–357 (2003).
13. White, R. J., Ghez, A. M., Reid, I. N. & Schultz, G. A test of pre-main-sequence evolutionary models across the stellar/substellar boundary based on spectra of the young quadruple GG Tauri. *Astrophys. J.* **520,** 811–821 (1999).
14. Dutrey, A., Guilloteau, S. & Simon, M. Images of the GG Tauri rotating ring. *Astron. Astrophys.* **286,** 149–159 (1994).
15. Piétu, V., Gueth, F., Hily-Blant, P., Schuster, K.-F. & Pety, J. High resolution imaging of the GG Tauri system at 267 GHz. *Astron. Astrophys.* **528,** A81 (2011).
16. Skemer, A. J. *et al.* Dust grain evolution in spatially resolved T Tauri binaries. *Astrophys. J.* **740,** 43 (2011).
17. Artymowicz, P., Clarke, C. J., Lubow, S. H. & Pringle, J. E. The effect of an external disk on the orbital elements of a central binary. *Astrophys. J.* **370,** L35–L38 (1991).
18. Beust, H. & Dutrey, A. Dynamics of the young multiple system GG Tauri. I. Orbital fits and inner edge of the circumbinary disk of GG Tau A. *Astron. Astrophys.* **439,** 585–594 (2005).
19. Pierens, A. & Nelson, R. P. On the migration of protoplanets embedded in circumbinary disks. *Astron. Astrophys.* **472,** 993–1001 (2007).
20. Pierens, A. & Nelson, R. P. Migration and gas accretion scenarios for the Kepler 16, 34, and 35 circumbinary planets. *Astron. Astrophys.* **556,** A134 (2013).
21. Guilloteau, S., Dutrey, A. & Simon, M. G. G. Tauri: the ring world. *Astron. Astrophys.* **348,** 570–578 (1999).
22. Dutrey, A. *et al.* Physical and chemical structure of planet-forming disks probed by millimeter observations and modeling. Preprint at http://arXiv.org/abs/1402.3503 (2014).
23. Delorme, P. *et al.* Direct-imaging discovery of a 12–14 Jupiter-mass object orbiting a young binary system of very low-mass stars. *Astron. Astrophys.* **553,** L5 (2013).
24. Duchêne, G. & Kraus, A. Stellar multiplicity. *Annu. Rev. Astron. Astrophys.* **51,** 269–310 (2013).

Acknowledgements ALMA is a partnership of ESO (representing its member states), NSF (USA) and NINS (Japan), together with NRC (Canada) and NSC and ASIAA (Taiwan), in cooperation with the Republic of Chile. The Joint ALMA Observatory is operated by ESO, AUI/NRAO and NAOJ. IRAM is supported by INSU/CNRS (France), MPG (Germany) and IGN (Spain). A.D. thanks the French programmes PNP, PCMI, PNPS and ASA for providing funding for this study.

Author Contributions A.D. led the project and participated in data reduction. All authors contributed to the data analysis, discussed the results and commented on the manuscript.

Author Information This paper makes use of the following ALMA data: ADS/JAO.ALMA2011.0.00059. Reprints and permissions information is available at www.nature.com/reprints. The authors declare no competing financial interests. Readers are welcome to comment on the online version of the paper. Correspondence and requests for materials should be addressed to A.D. (Anne.Dutrey@obs.u-bordeaux1.fr).

METHODS

ALMA observations. GG Tau was observed with ALMA in Cycle 0 (project 2011.0.00059.S) in Band 9 on August 13 2012. The spectral set-up was of 4 spectral windows of total width 0.938 GHz, centred at 691.485, 689, 676 and 674 GHz respectively. The correlator observed in dual polarization, yielding a channel spacing of 244 kHz, or 0.11 km s^{-1}. With Hanning smoothing, the spectral resolution is twice those values. The array of 23 antennas was in its extended configuration. The water vapour was about 0.25 mm and system temperatures ranged from 500 to 1,000 K. Comparison of the CO data with existing ^{12}CO $J = 2$–1 IRAM data (Fig. 1) revealed a frequency shift of the ALMA observations whose origin could not be identified. We corrected the velocity offset by correlating with the IRAM data. The velocity difference was 0.97 ± 0.01 km s^{-1}. Since it is an offset, it does not introduce any error on the velocity gradient. The absolute flux scale was determined using Ceres. The ALMA data were calibrated using CASA then exported through UVFITS to be imaged and analysed using GILDAS. Extended Data Fig. 1 presents the resulting channel maps.

The integrated ring+disk continuum flux is in good agreement with the previous unresolved detection[25]: no more than 20% of the flux is lost.

For the CO $J = 6$–5 line, we only recover a fraction of the integrated line flux of $\sim 38 \pm 8$ Jy km s^{-1} (ref. 26). The ALMA antenna configuration exhibits a lack of short baselines which induces a partial loss of flux for the extended structures that deconvolution cannot recover, particularly in the CO circumbinary disk which extends up to 800 AU. We ran several disk simulations of the CO $J = 6$–5 emission using the ALMA simulator[27]. If emission only arises from the ring, our simulation shows that about 20% of the emission would be filtered out by the configuration of ALMA. A much larger fraction is lost if CO $J = 6$–5 extends into the whole outer disk (up to 800 AU); this fraction depends on the signal to noise ratio. The expected extension of the CO $J = 6$–5 emission depends on the excitation conditions in the outer disk, so uncertainties on the amount of flux loss preclude any quantitative analysis of the large scale disk emission in CO $J = 6$–5 data.

IRAM data. We complement ALMA data with CO $J = 2$–1 and continuum images from the IRAM interferometer. The compact configuration was used for observations on 5–6 December 1997, and long baselines up to 400 m were used on 28–31 January 1998 and 18 March 1998[11]. The unpublished extended configuration data were obtained on 16 February 2008. System temperatures were 120 K. Flux calibration, based on MWC349, gives an absolute flux accuracy of about 10%. Imaging was performed using GILDAS software. The resulting beam size is $0.65'' \times 0.29''$ at position angle PA = 21°. The spectral resolution is 0.10 km s^{-1}, and the effective noise is about 14 mJy per beam (up to 20 mJy per beam on the channels with the most extended emission due to deconvolution limits). The continuum image at 1.3 mm was produced using line-free channels. Its effective noise is limited by dynamic range to about 1 mJy per beam. Extended Data Fig. 2 shows the CO $J = 2$–1 channel maps.

Proper motions. Accounting for the expected orbital motion, we adopted proper motions of (17, −19) mas yr^{-1} for the centre of mass of the system[28] to merge all data.

Inner dust disk properties. For the disk of GG Tau Aa, the total fluxes of 55 mJy at 0.45 mm and 10 mJy at 1.3 mm are consistent with optically thick dust emission at a mean temperature of ~35 K (ref. 29) and an outer radius of the order of 7 AU, a size in agreement with tidal truncation by GG Tau Ab. Assuming a standard dust opacity of 0.02 cm^2 g^{-1} at 1.3 mm, the minimum disk mass is roughly $10^{-3}\,M_\odot$ or a Jupiter's mass worth of gas and dust. The rate at which matter is accreting from the disk onto the surface of GG Tau Aa is in the range $(\sim 10^{-7.56}$–$10^{-8.02})\,M_\odot$ yr^{-1} (ref. 12). Such a disk would dissipate in less than $\sim(3 \times 10^4)$–10^5 yr without external replenishment. We place an upper limit on the circumstellar disk mass surrounding GG Tau Ab of $\sim 10^{-5}\,M_\odot$ at 3σ (a little more than one Earth mass) or an upper limit on its radius of ~1 AU by extrapolating the dust opacity to 0.45 mm, 0.067 cm^2 g^{-1}, and using a similar temperature as in the disk of GG Tau Aa. This is consistent with the separation of Ab1 and Ab2 of ~4.5 AU (ref. 8).

Inner cavity. CO excitation conditions. We performed escape probability calculations using the code RADEX[30] (http://www.sron.rug.nl/~vdtak/radex/radex.php), a radiative transfer code dedicated to calculations of molecular line excitations. At the location of the eastern CO $J = 2$–1 peak (~80 AU from the stars), the CO lines are optically thick, H_2 densities must be greater than 10^5 cm^{-3}, and the gas is cold with a temperature in the range ~30–40 K. Closer to the stars, the peaks of the bright CO $J = 6$–5 regions correspond to optically thin emission, with a warmer temperature of about 70 K and a H_2 density of $\sim 5 \times 10^5$ cm^{-3}. These densities agree with the pre-shock gas densities derived from shock models for the 2.12-μm H_2 emission maps. With a standard CO/H_2 ratio of 10^{-4}, the mass of each optically thin clump is of the order of $\sim(3$–$7) \times 10^{-5}\,M_\odot$.

CO velocity field. We studied the velocity variations of the CO $J = 6$–5 emission. The spectra displayed in Extended Data Fig. 3, at the locations of the CO $J = 6$–5 clumps, also show that the velocity is dominated by rotation. The complexity of the system (which is triple) and the quality of the data preclude any detailed modelling of the velocity field, but some points can be addressed. From a compilation of existing values in the literature, we derive for GG Tau Aa a velocity of 5.8 ± 0.2 km s^{-1} (ref. 31). This implies a difference of the order of 0.6 ± 0.2 km s^{-1} from the known systemic (barycentric) velocity of the whole stellar system[21]. Extended Data Fig. 3 reveals that the measured CO gas velocity near GG Tau Aa is in very good agreement with Aa velocity as expected for bound motions. Around the disk minor axis, we note that the isovelocity contours are twisted at a radius of about 70–80 AU from the mass centre. Inside this radius, the isocontours are closely packed, and suddenly spread out beyond. Furthermore, the isovelocity contours are aligned on the Aa–Ab line between GG Tau Aa and Ab. This is exactly what is expected when the gravitation field, externally dominated by the total stellar mass ($1.28\,M_\odot$), becomes dominated by the individual mass of the star Aa and binary Ab. At the location of the CO $J = 6$–5 clumps, the spectra displayed in Extended Data Fig. 3 also exhibit a large velocity dispersion ($\delta v \approx 2$–2.5 km s^{-1}) which could be partly due to infall. We check this by analysing the velocity field along the minor axis at the northern clump. In an inclined disk, projected velocities due to infall are at a maximum along the minor axis, contrary to rotation velocities which are at a maximum along the major axis[32,33]. Taking into account the beam size of 35 AU, we find that the maximum velocity dispersion along the minor axis in a spectrum would be of the order 1.2 km s^{-1} if it is only due to Keplerian rotation around central objects of $0.65\,M_\odot$ (because this CO $J = 6$–5 clump is located in the area where the velocity field is dominated by GG Tau Ab). This is a factor two lower than the observed line widths of 2–2.5 km s^{-1}. In disks, turbulence cannot explain such a large dispersion[34]. However, infall velocities can be $\sqrt{2}$ larger than Keplerian velocities. It is therefore reasonable to conclude that the observed velocities and line widths are compatible with a combination of rotation and infall. For the southern clump, located near GG Tau Aa, the velocity profile is very complex. For instance, the spectrum of the Aa star shows two double peaked profiles, perfectly centred on the velocity of Aa (5.8 km s^{-1}), but with significantly different widths (full-width at half-maximum, FWHM, ~1.5 and 6 km s^{-1}). The total velocity dispersion of the broader double peaked profile (~6 km s^{-1}) is compatible with a circumstellar disk of outer radius of the order of ~20 AU (ref. 35), if the inclination of the system is the same as that of the outer ring (35°). Such a CO outer radius is compatible with the value derived from the dust (provided a small part of the dust emission is optically thin) and tidal truncation due to GG Tau Ab (the physical star separation being about 42 AU).

Outer disk. Dust ring properties. We use Diskfit, a radiative transfer code dedicated to the modelling of the disk images in mm/submm regime[36], to analyse the dust properties inside the outer ring using the best data available (3 mm and 1.3 mm PdBI data and 0.45 mm ALMA observations). A modified Levenberg-Marquardt scheme with step adjustment is used to derive the best fit[37]. The analysis is performed in the Fourier plane to avoid non linear effects due to the deconvolution. We explore large ranges for all parameters to avoid local minima. Extended Data Fig. 4 and Extended Data Table 2 present the results, with 1σ formal error bars derived from the covariance matrix. The errors are computed on the basis of the difference between data and model, so include dynamic range limitations in addition to thermal noise. We use simple truncated power laws to model the surface density and temperature. We allow dust emissivity κ_ν to vary with frequency as $\kappa_\nu = \kappa_o \times (\nu/\nu_o)^\beta$ (β being the emissivity index). Such a simple model is valid for the dust distribution since the emission is known to be confined in a ring with sharp edges[9,21]. The derived geometrical parameters are in very good agreement with the previous results[21]. Since the dust temperature is mostly constrained by the ratio of the flux density at 0.45 mm and 1.3 mm, we checked that the results remain robust even assuming an absolute flux calibration error as high as 20% at 0.45 mm. The density, temperature and dust spectral index are robust with respect to all minimizations. However, we find a slight dependence between β and the surface density. This is not surprising because in the optically thin case, the brightness temperature is proportional to $\tau \propto \kappa(0.45\,\mathrm{mm}) \times \Sigma(r)$ (with $\kappa(0.45\,\mathrm{mm})$ the absorption coefficient of the dust at 0.45 mm). A better removal of this dependence would require higher angular resolution at 1.3 mm. We found a value for the emissivity index $\beta = 1.0 \pm 0.1$, which indicates moderate grain growth compared to interstellar dust. Such a grain growth is compatible with a recent analysis of the dust ring performed between 7 and 1.3 mm[9]. We found a marginal dependency of β with radius, suggesting that larger dust particles reside near the inner edge of the outer disk (that is, closer to the central stars), as observed for some circumstellar disks orbiting young single stars[38]. So far, dust temperatures have been derived either from Monte-Carlo dust disk models[39] or one-dimensional thermal models associated with pure mm data[9]. In our case, we are able to directly derive the dust temperature thanks to the deviation from the Rayleigh Jeans regime at 0.45 mm, combined with sufficiently high spatial resolution at 0.45 mm and 1.3 mm. This permits the removal of the degeneracy between the temperature and the opacity. This direct

measurement is of great interest for a better characterization of disk mid-planes where planet formation is expected to occur.

CO excitation conditions. Analysis of the physical conditions in the outer ring at radius around 200 AU shows that the mid-plane H_2 density ($\sim 10^9$ cm^{-3}) is high enough to thermalize CO transitions up to $J = 6$–5[21]. Excitation of the CO $J = 6$–5 line requires a H_2 critical density of $\sim 3 \times 10^5$ cm^{-3}. We also derive a dust temperature lower than the CO freeze-out temperature of 17 K. Therefore the observed large scale emissions from the CO $J = 1$–0 and $J = 2$–1 transitions must arise from a warmer molecular layer located above the mid-plane, as predicted by layered disk models[22] and revealed by ALMA observations of HD 163296[40].

Using our measurement of the dust temperature, we find that the hydrostatic scale height of the gas and dust is about ~25 and ~35 AU at radii of 200 and 300 AU, respectively. If the CO gas originates in a layer located at about 3 scale heights (in agreement with chemical models), and taking into account the vertical temperature gradient, the H_2 density would be $\sim 10^5$ and $\sim 10^4$ cm^{-3} at radii of 200 and 300 AU, respectively. This is sufficient to thermalize the $J = 1$–0 and $J = 2$–1 lines, but not the $J = 6$–5 transition, which can be partially subthermally excited outside the ring. Note that any gap at the outer edge of the ring created by an embedded protoplanet (see section below) would imply some subthermal excitation there.

A CO hotspot at the outer edge of the ring. The CO $J = 6$–5 and $J = 2$–1 maps reveal a brightness enhancement of unknown origin near the outer edge of the dust ring (Fig. 1 and spectrum in Extended Data Fig. 3). From the CO $J = 2$–1 emission which is optically thick and thermalized, we derive a minimum temperature of ~40 K in this clump. This indicates a temperature enhancement of at least 20 K compared to the surrounding optically thick CO gas. The feature is clearly dominated by the gas emission, unlike the recent detection of a dusty vortex-like structure, or dust trap, in the circumstellar disk associated with Oph IRS 48[41]. In the high angular resolution continuum maps at 0.45 mm and 1.3 mm, there is no dust counterpart to this bright CO peak. The dust absorption coefficient being small, only a sufficiently large and massive dust clump would be detectable. Given the effective (dynamic range limited) noise, the (dust) mass limit is a few times $10^{-7}\,M_\odot$ at 3σ, or the size must be smaller than about 4 AU, assuming a dust temperature of 40 K. In Extended Data Fig. 3, there is a marginal excess emission at 1.3 mm (4σ level) in the difference map (right panel) at the location of the blob. This has to be taken with caution since there are other 4σ peaks which are likely to trace some extended cold emission beyond the ring outer radius[21]. Analysis of the GG Tau A dust ring in term of a dust trap, based on resolved images between 7 and 1.3 mm, has been recently achieved but remains inconclusive[9]. The presence 10″ away of the binary star GG Tau B could induce gravitational disturbances in the circumbinary disk especially if its orbit is eccentric[42]. However, the total mass of GG Tau B is very low (~0.17 $M_\odot$; ref. 13) and it is located far away from the GG Tau A circumbinary ring (~1,400 AU). Therefore, we conclude that it is unlikely that GG Tau B would have induced such a sizeable disturbance in the circumbinary ring. We explore here another interesting possibility; this feature would be indirect evidence for an unknown (already formed) embedded companion that is still actively accreting material from the circumbinary disk[43]. In this scenario, the planet remains undetectable at millimetre wavelengths but the warmer accreting envelope can be seen[44,45]. The presence of such a companion would provide an explanation for the mass confinement in a narrow ring (~ 80% of the circumbinary mass is located within the ~90 AU breadth ring[21]). This situation is similar to the gas free, dusty ring orbiting the more evolved star Fomalhaut, where confinement by shepherding planets appears to be the most consistent explanation[46].

Simulations of the evolution of Kepler systems where exoplanets have been observed reveal that Saturn-like planets are expected to migrate to reach the 4:1 resonance[20] without opening a gap, except if the disk is very cold, as is the case for the GG Tau ring. In such cold disks, a protoplanet can remain at the ring's outer edge and the size of the gap will mainly depend on the planet mass[20]. So far, we have not detected a gap in the gas and dust circumbinary distribution of GG Tau A. Our CO $J = 6$–5 map shows that there is almost no CO $J = 6$–5 emission located outside the outer ring; this is expected if there is a gap or a strong density decrease which implies subthermal excitation. Gap opening depends on several physical parameters, such as the mass of the planet, and the disk viscosity and aspect ratio[47]. For example, a Saturn-like body located at 250 AU in the circumbinary disk would open a gap of about 35 AU assuming standard viscosity ($\alpha = 10^{-2}$) and aspect ratio $h(r)/r = 0.1$. Under the same physical conditions, the gap would be only 12 AU wide for a Neptune-like planet[48]. Observing a gap in the existing CO $J = 2$–1 map would be difficult because the CO $J = 2$–1 line is very optically thick, making the expected ring/gap brightness contrast difficult to detect, except if the gap is very deep with a high ring/gap density contrast (larger than the CO opacity), and is large enough to be directly seen (about 40 AU given the beam size). ^{13}CO is less optically thick (by a factor of 70) but the existing ^{13}CO $J = 2$–1 map[21] has an angular resolution ($0.88 \times 0.56''$ or 120×80 AU) insufficient for direct imaging. However, a ring/outer disk density contrast of ~25 at 260 AU has been reported[21]. This contrast could be the signature of an unresolved gap in the ^{13}CO $J = 2$–1 map. A spectroscopic detection[49] would be possible only by using very high sensitivity data, which do not exist so far. Very sensitive observations of optically thinner CO isotopologues at high angular resolution ($\ll 0.1 - 0.2''$) are needed to study the hot spot's properties (including the viewing of a gap) and its implications for planet formation scenarios.

25. Moriarty-Schieven, G. H. & Butner, H. M. A submillimeter-wave "flare" from GG Tauri? *Astrophys. J.* **474,** 768–773 (1997).
26. Thi, W.-F., van Dishoeck, E. F., Blake, G. A., van Zadelhoff, G.-J. & Hogerheijde, M. R. Detection of H_2 pure rotational line emission from the GG Tauri binary system. *Astrophys. J.* **521,** L63–L66 (1999).
27. Pety, J., Gueth, F. & Guilloteau, S. ALMA+ACA simulation tool. *ALMA Memo* **386,** 1–10 (2002).
28. Ducourant, C. *et al.* Pre-main sequence star proper motion catalogue. *Astron. Astrophys.* **438,** 769–778 (2005).
29. Piétu, V., Guilloteau, S., Di Folco, E., Dutrey, A. & Boehler, Y. Faint disks around classical T Tauri stars: small but dense enough to form planets. *Astron. Astrophys.* **564,** A95 (2014).
30. van der Tak, F. F. S., Black, J. H., Schöier, F. L., Jansen, D. J. & van Dishoeck, E. F. A computer program for fast non-LTE analysis of interstellar line spectra. With diagnostic plots to interpret observed line intensity ratios. *Astron. Astrophys.* **468,** 627–635 (2007).
31. Nguyen, D. C., Brandeker, A., van Kerkwijk, M. H. & Jayawardhana, R. Close companions to young stars. I. A large spectroscopic survey in Chamaeleon I and Taurus-Auriga. *Astrophys. J.* **745,** 119 (2012).
32. Guilloteau, S. & Dutrey, A. Physical parameters of the Keplerian protoplanetary disk of DM Tauri. *Astron. Astrophys.* **339,** 467–476 (1998).
33. Rosenfeld, K. A., Chiang, E. & Andrews, S. M. Fast radial flows in transition disk holes. *Astrophys. J.* **782,** 62 (2014).
34. Guilloteau, S. *et al.* Chemistry in disks. VIII. The CS molecule as an analytic tracer of turbulence in disks. *Astron. Astrophys.* **548,** A70 (2012).
35. Beckwith, S. V. W. & Sargent, A. I. Molecular line emission from circumstellar disks. *Astrophys. J.* **402,** 280–291 (1993).
36. Boehler, Y., Dutrey, A., Guilloteau, S. & Piétu, V. Probing dust settling in proto-planetary discs with ALMA. *Mon. Not. R. Astron. Soc.* **431,** 1573–1586 (2013).
37. Piétu, V., Dutrey, A. & Guilloteau, S. Probing the structure of protoplanetary disks: a comparative study of DM Tau, LkCa 15, and MWC 480. *Astron. Astrophys.* **467,** 163–178 (2007).
38. Guilloteau, S., Dutrey, A., Piétu, V. & Boehler, Y. A dual-frequency sub-arcsecond study of proto-planetary disks at mm wavelengths: first evidence for radial variations of the dust properties. *Astron. Astrophys.* **529,** A105 (2011).
39. Madlener, D., Wolf, S., Dutrey, A. & Guilloteau, S. The circumstellar disk of HH 30. Searching for signs of disk evolution with multi-wavelength modeling. *Astron. Astrophys.* **543,** A81 (2012).
40. de Gregorio-Monsalvo, I. *et al.* Unveiling the gas-and-dust disk structure in HD 163296 using ALMA observations. *Astron. Astrophys.* **557,** A133 (2013).
41. van der Marel, N. *et al.* A major asymmetric dust trap in a transition disk. *Science* **340,** 1199–1202 (2013).
42. Beust, H. & Dutrey, A. Dynamics of the young multiple system GG Tauri. II. Relation between the stellar system and the circumbinary disk. *Astron. Astrophys.* **446,** 137–154 (2006).
43. Gressel, O., Nelson, R. P., Turner, N. J. & Ziegler, U. Global hydromagnetic simulations of a planet embedded in a dead zone: gap opening, gas accretion, and formation of a protoplanetary jet. *Astrophys. J.* **779,** 59 (2013).
44. Wolf, S., Gueth, F., Henning, T. & Kley, W. Detecting planets in protoplanetary disks: a prospective study. *Astrophys. J.* **566,** L97–L99 (2002).
45. Wolf, S. & D'Angelo, G. On the observability of giant protoplanets in circumstellar disks. *Astrophys. J.* **619,** 1114–1122 (2005).
46. Boley, A. C. *et al.* Constraining the planetary system of Fomalhaut using high-resolution ALMA observations. *Astrophys. J.* **750,** L21 (2012).
47. Crida, A., Morbidelli, A. & Masset, F. On the width and shape of gaps in protoplanetary disks. *Icarus* **181,** 587–604 (2006).
48. Takeuchi, T., Miyama, S. M. & Lin, D. N. C. Gap formation in protoplanetary disks. *Astrophys. J.* **460,** 832–847 (1996).
49. Dutrey, A. *et al.* Cavities in inner disks: the GM Aurigae case. *Astron. Astrophys.* **490,** L15–L18 (2008).

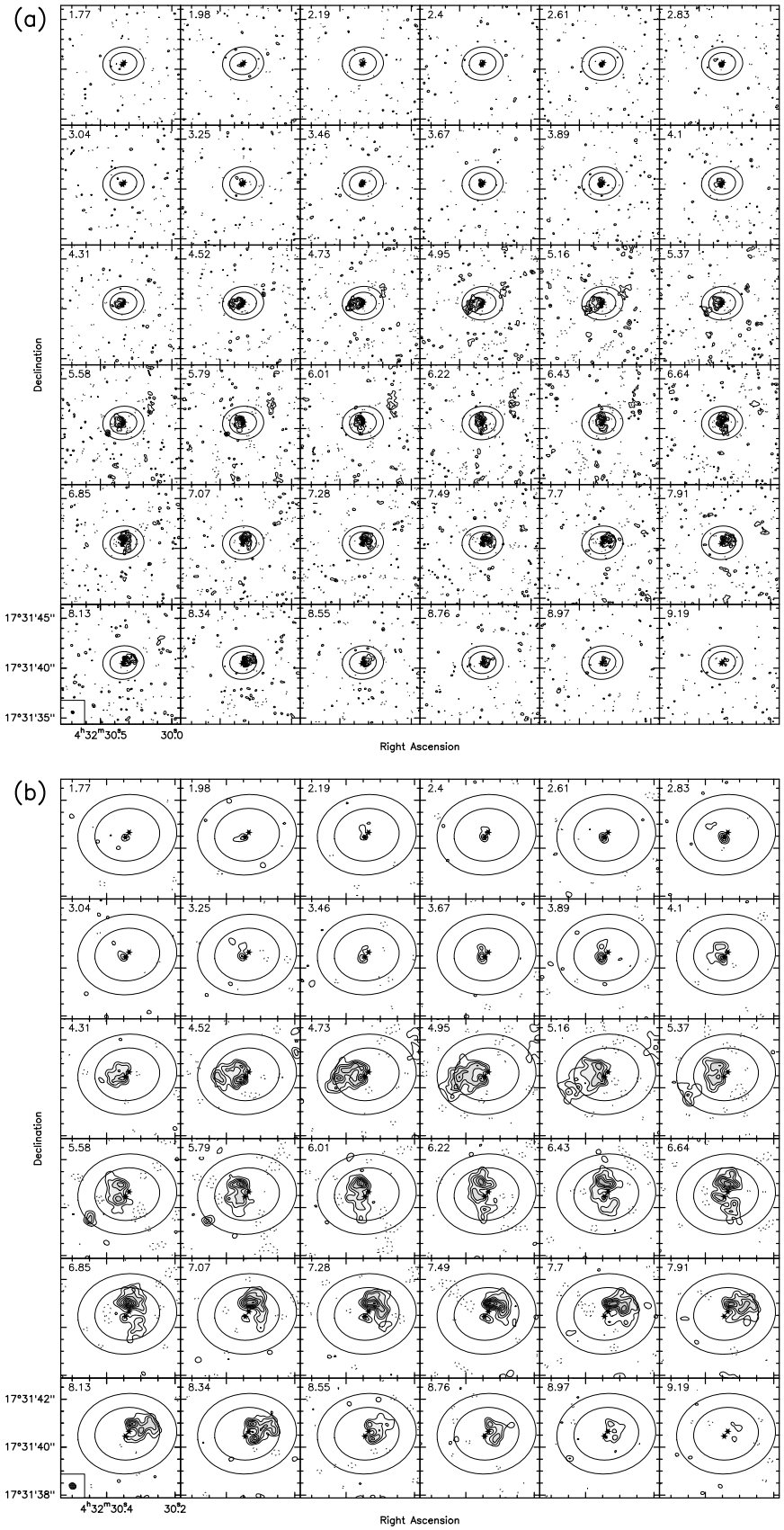

Extended Data Figure 1 | ALMA CO $J = 6$–5 velocity channel map. For each spectroscopic channel, the velocity is given at top left. **a**, Full map; **b**, inner zoom. The beam size is $0.29'' \times 0.25''$ at PA 68°. The level step is 100 mJy per beam or 3.51 K corresponding to 3.4σ.

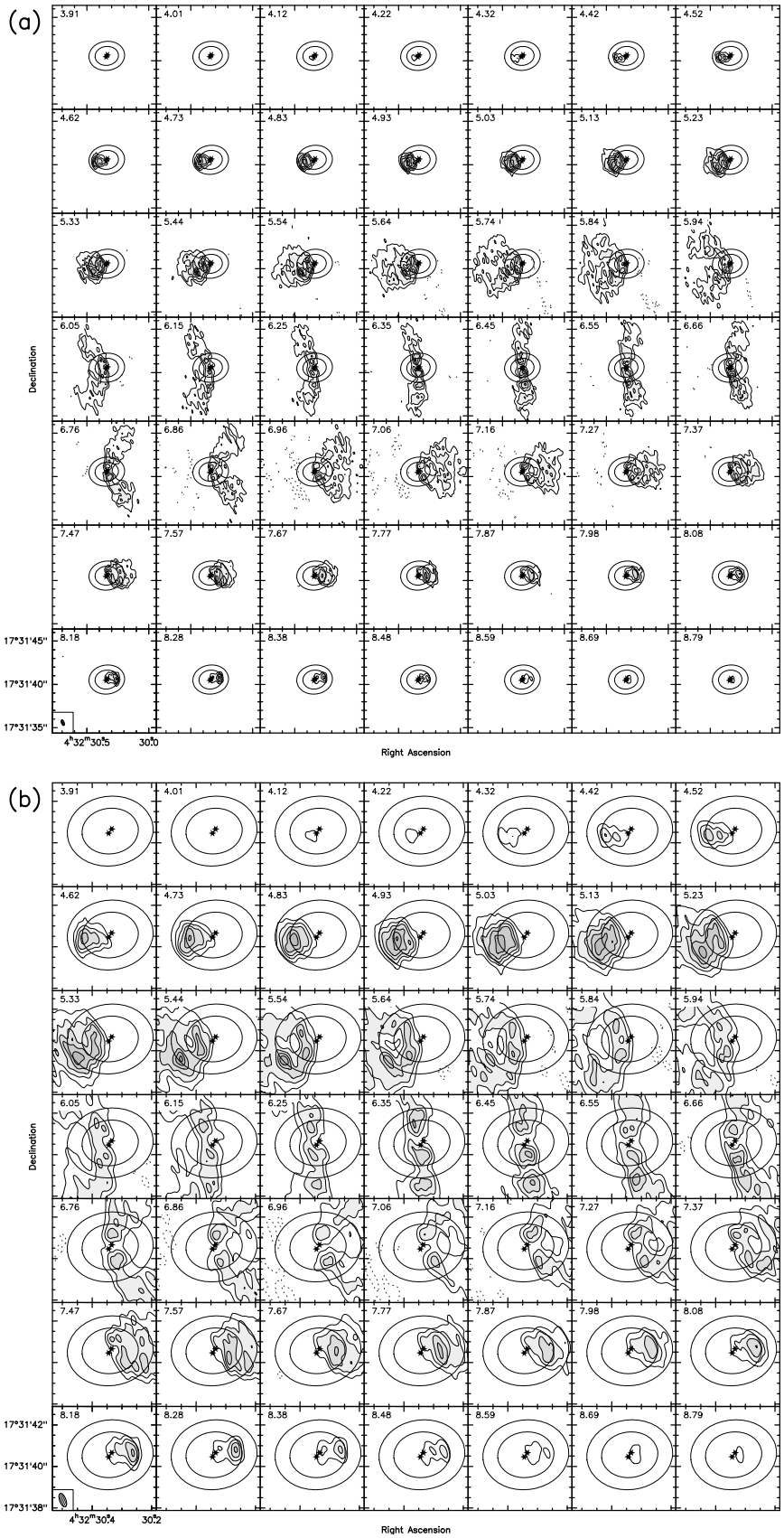

Extended Data Figure 2 | IRAM CO $J = 2–1$ velocity channel map. For each spectroscopic channel, the velocity is given at top left. **a**, Full map; **b**, inner zoom. The beam size is $0.68'' \times 0.31''$ at PA 21°. The level step is 50 mJy per beam or 5.48 K corresponding to 3.85σ.

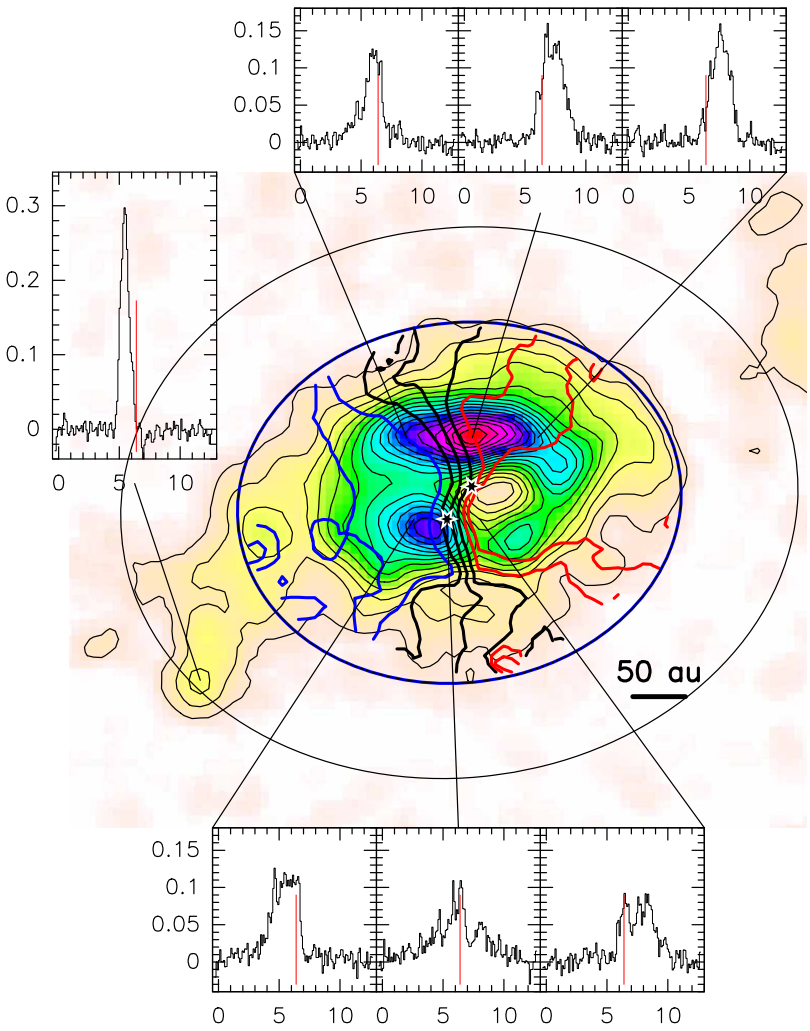

Extended Data Figure 3 | Montage of the CO $J = 6–5$ data. False colours and black contours show the integrated area. The velocity gradient is given in thick contours: blue (gas approaching), black (systemic velocity) and red (gas receding). Stars show the location of Aa (south) and Ab (north). The two large ellipses show the ring edges. The three spectra sets (y axis, intensity in units of Jy per beam; x axis, velocity in units of km s^{-1}) show the velocity gradient along the northern/southern CO $J = 6–5$ clump, respectively (dominated by rotation). On spectra, the red line is the systemic velocity (6.4 km s^{-1}). From east to west, the black contours correspond to velocity contours of 6.0, 6.4 and 6.8 km s^{-1}. The systemic velocity contour passes between the two stars (barycentre). The single spectrum corresponds to the location of the hotspot.

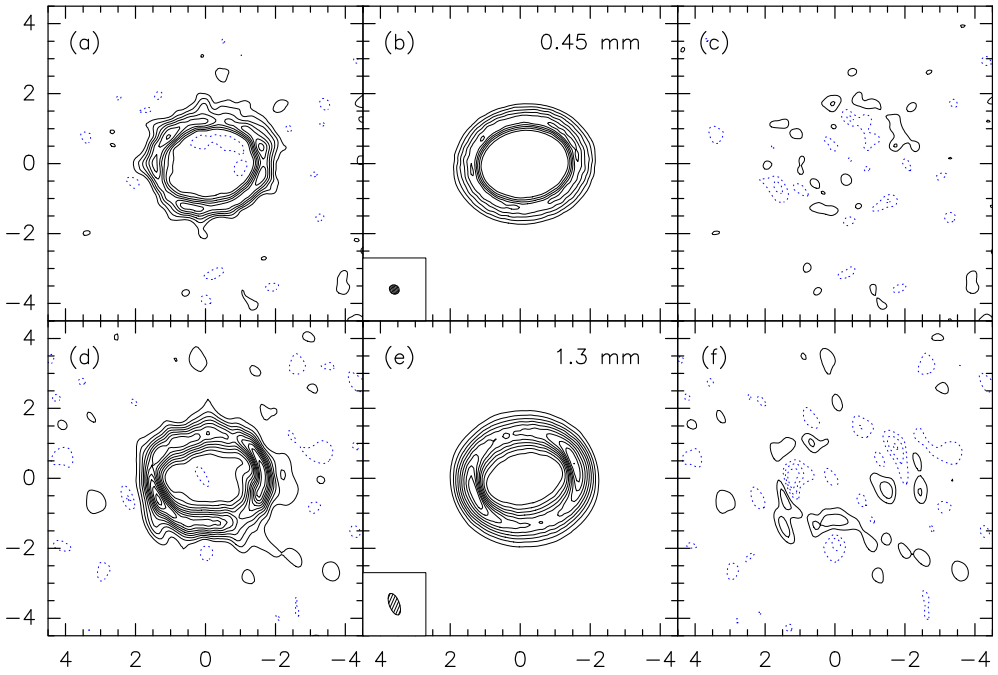

Extended Data Figure 4 | Dust ring best model. **a**, ALMA continuum data at 0.45 mm (emission from Aa circumstellar disk has been removed). **b**, Best model at 0.45 mm, same contour levels. **c**, Difference between the observations and the best model, contour levels correspond to 2σ. **d**, **e**, **f**, As **a**, **b**, **c** but for the IRAM continuum data at 1.3 mm.

Extended Data Table 1 | Parameters relevant to the analysis of the ALMA data

CO J=2-1 analysis			
Systemic velocity	$V_{\rm LSR}$	$6.38 \pm$	0.02 km.s^{-1}
Orientation	PA	$7 \pm$	2°
Inclination	i	$37 \pm$	1°
Disk outer radius	$R_{\rm out}$	~ 800	au
Velocity law:	$V(r) = V_{100}(\frac{r}{100\rm au})^{-v}$		
velocity at 100 au	V_{100}	$3.4 \pm$	0.1 km.s^{-1}
exponent	v	$0.5 \pm$	0.1

Values are adopted from previous work (see Methods).

Extended Data Table 2 | Best fit results for the GG Tau circumbinary dust disk, as derived from the whole continuum data set

Geometry		
Orientation	PA	$6.5 \pm 0.2°$
Inclination	i	$35.0 \pm 0.2°$
Size		
Ring inner radius	R_i	193 ± 1 au
Ring outer radius	R_o	285 ± 1 au
Surface density law: $\Sigma(r) = \Sigma_{200}(\frac{r}{200\mathrm{au}})^{-p}$		
H_2 surface density	Σ_{200}	$9 \pm 1\ 10^{24}$ cm^{-2}
exponent	p	1.3 ± 0.2
Temperature law: $T(r) = T_{200}(\frac{r}{200\mathrm{au}})^{-q}$		
Dust Temperature	T_{200}	13.8 ± 0.3 K
exponent	q	1.1 ± 0.1
Gas-to-Dust Ratio	G/D	100 -
Absorption Coefficient (gas+dust)	$\kappa(1.3\,mm)$	0.02 cm^2/g -
Dust Spectral Index	β	1.0 ± 0.1